



The crack tip fields in strain gradient plasticity: the asymptotic and numerical analyses

J.Y. Chen^a, Y. Wei^b, Y. Huang^{c,*}, J.W. Hutchinson^b, K.C. Hwang^d

^a*Department of Mechanical Engineering — Engineering Mechanics, Michigan Technical University, Houghton, MI 49931, USA*

^b*Division of Engineering and Applied Sciences, Harvard University, Cambridge, MA 02138, USA*

^c*Department of Mechanical and Industrial Engineering, University of Illinois, Urbana, IL 61801, USA*

^d*Department of Engineering Mechanics, Tsinghua University, Beijing 100084, People's Republic of China*

Received 1 December 1998; received in revised form 31 July 1999; accepted 31 July 1999

Abstract

An investigation of asymptotic crack tip singular fields and their domain of validity is carried out for mode I cracks in solids characterized by the phenomenological strain gradient plasticity theory proposed by Fleck NA, Hutchinson JW. (Strain gradient plasticity. In: Hutchinson JW, Wu TY, editors. *Advances in applied mechanics*, vol. 33. New York: Academic Press, 1997. pp. 295–361.) Separable near-tip singular fields are determined where fields quantities depend on the radial and circumferential coordinates (r, θ) according to $r^p f(\theta)$. The singular field is completely dominated by the strain gradient contributions to the constitutive law. In addition to the asymptotic analysis, full field numerical solutions are obtained by a finite element method using elements especially suited to the higher order theory. It is found that the singular field provides a numerically accurate representation of the full field solution only within a distance from the tip that is a tiny fraction of the constitutive length parameter. The constitutive theory itself is not expected to be valid in this domain. Curiously, the normal traction acting across the extended crack line ahead of the crack tip is found to be compressive in the singular field. The conclusion which must be drawn is that the singular field has a tiny domain of mathematical validity (neglecting crack face interaction), but no domain of physical validity. The significant elevation of tractions ahead of the crack tip due to strain gradient hardening occurs at distances from the crack tip which are well outside this tiny domain in a region where the plasticity theory is expected to be applicable. The asymptotic singular fields are incapable of capturing the effect of traction elevation. © 1999 Elsevier Science Ltd. All rights reserved.

Keywords: Asymptotic crack tip fields; Strain gradient plasticity

* Corresponding author. Tel.: +1-217-265-5072; fax: +1-217-244-6534.

E-mail address: huang9@uiuc.edu (Y. Huang).

1. Introduction

Attempts to link macroscopic fracture behavior to atomistic fracture processes are frustrated by the inability of classical plasticity theories to model stress–strain behavior adequately at the small scales involved in crack tip deformation. For example, in a remarkable series of experiments, Elssner et al. [1] measured both the macroscopic fracture toughness and atomic work of separation of an interface between a single crystal of niobium and a sapphire single crystal. The macroscopic fracture toughness was measured using a four-point bending specimen designed for the determination of interfacial toughness, while the atomic value was inferred from the equilibrium shape of microscopic pores on the interface. The macroscopic fracture toughness was 2–3 orders of magnitude higher than the atomic work of separation because of the large amount of plastic flow in niobium. On the other hand, the interface crack tip remained atomistically sharp, i.e., it was not blunted even though niobium had a large number of dislocations. The stress level needed to produce atomic decohesion of a lattice or a strong interface is typically of the order of 0.03 times the Young's modulus, or 10 times the tensile yield stress. However, as Hutchinson [2] pointed out, the stress level that can be achieved near a crack tip is not larger than 4–5 times the yield stress according to the models based on classical plasticity theories. This clearly falls short of triggering the atomic decohesion observed in Elssner et al's [1] experiments.

The strain gradient plasticity theories may provide such a link between macroscopic fracture behavior and atomistic fracture processes. The theories have been developed for application to materials and structures whose dimension controlling plastic deformation falls roughly between 0.1 and 10 microns (e.g., [3–7]). Within this range of microns and submicrons, metals require significantly higher stresses to induce plastic deformation than at larger macroscopic scales. This significant elevation in stresses has been observed in many small-scale experiments, such as micro-indentation and nano-indentation [8–13], micro-torsion [5] and micro-bending [14]. This increase in stress level comes from the storage of geometrically necessary dislocations at the microscale [15–17], which causes materials to further work harden in addition to plastic work hardening from statistically stored dislocations. The geometrically necessary dislocations are directly related to the local curvature of deformation, or equivalently strain gradients (e.g., [5,6,17], which is the reason that strain gradient appears in the constitutive model of microscale (strain gradient) plasticity.

There are several theories of strain gradient plasticity. Fleck and Hutchinson [3] and Fleck et al. [5] developed a phenomenological theory of strain gradient plasticity based on the rotation gradients of deformation. Fleck and Hutchinson [4] further extended the phenomenological theory to include both stretch gradients and rotation gradients of deformation. An alternative formulation of strain gradient plasticity was proposed by Gao et al. [6] and Huang et al. [7], which was derived from Taylor's dislocation model and a multiscale approach to connect strain gradients with the density of geometrically necessary dislocations.

Strain gradient effects are important near a crack tip due to the crack tip singularity. There are some studies on the asymptotic crack tip fields [18–21] as well as full-field solutions [20,22] in rotation-gradient-based strain gradient plasticity. However, the anticipated significant elevation in stresses is not observed near the crack tip because the effect of stretch gradients has not been accounted for in their studies (e.g., [23,24]).

In order to account for both stretch gradients and rotation gradients of deformation, we use the phenomenological strain gradient plasticity theory [4] to investigate the asymptotic crack tip field and its domain of validity. We begin with a summary of the phenomenological strain gradient theory in Section 2. The asymptotic crack tip fields are obtained in Section 3, while a finite element method especially suite to the higher order continuum theory is used in Section 4 to determine the domain of validity of the asymptotic crack tip fields. It is found that the singular asymptotic crack tip field provides a numerically accurate representation of the full-field solution only within a distance from the tip that is a tiny fraction of the constitutive length parameter. The constitutive theory is not expected to be valid in this domain. It is concluded that the asymptotic field has a tiny domain of mathematical validity, but no domain of physical validity. The significant elevation in stresses due to strain gradient effects, however, occurs well outside this tiny domain and in a region where the plasticity theories are expected to be applicable.

2. Summary of the phenomenological strain gradient plasticity theory

2.1. The phenomenological strain gradient plasticity theory

The phenomenological strain gradient plasticity theory [4] includes both rotation gradients and stretch gradients of deformation. It is summarized in this section for plane-strain ($\epsilon_{33} = 0$) deformation theory.

The in-plane strains $\epsilon_{\alpha\beta}$ and strain gradients $\eta_{\alpha\beta\gamma}$ are related to displacements u_α by

$$\epsilon_{\alpha\beta} = \frac{1}{2}(u_{\alpha, \beta} + u_{\beta, \alpha}), \quad \alpha, \beta = 1, 2, \tag{1}$$

$$\eta_{\alpha\beta\gamma} = u_{\gamma, \alpha\beta}, \quad \alpha, \beta, \gamma = 1, 2. \tag{2}$$

Since the near-tip asymptotic field is dominated by plastic deformation, elastic deformation can be neglected such that the material is incompressible. This requires

$$\epsilon_{\alpha\alpha} = 0, \quad \eta_{\gamma\alpha\alpha} = 0, \quad \gamma = 1, 2. \tag{3}$$

The work conjugates of strains and strain gradients are (symmetric) stresses $\sigma_{\alpha\beta}$ ($= \sigma_{\beta\alpha}$, $\alpha, \beta = 1, 2$), and (symmetric) higher-order stresses $\tau_{\alpha\beta\gamma}$ ($= \tau_{\beta\alpha\gamma}$, $\alpha, \beta, \gamma = 1, 2$), respectively. For an incompressible solid, the constitutive law of the deformation theory of strain gradient plasticity can be written in terms of the strain energy density as W as

$$\sigma'_{\alpha\beta} = \frac{\partial W}{\partial \epsilon_{\alpha\beta}}, \quad \tau'_{\alpha\beta\gamma} = \frac{\partial W}{\partial \eta_{\alpha\beta\gamma}}, \quad \alpha, \beta, \gamma = 1, 2, \tag{4}$$

where $\sigma'_{\alpha\beta} = \sigma_{\alpha\beta} - \frac{1}{3}(\sigma_{\delta\delta} + \sigma_{33})\delta_{\alpha\beta}$, $\alpha, \beta = 1, 2$ are deviatoric stresses, $\tau'_{\alpha\beta\gamma} = \tau_{\alpha\beta\gamma} - \frac{1}{4}[(\tau_{\alpha\delta\delta} + \tau_{\alpha 33})\delta_{\beta\gamma} + (\tau_{\beta\delta\delta} + \tau_{\beta 33})\delta_{\alpha\gamma}]$, $\alpha, \beta, \gamma = 1, 2$ are deviatoric higher-order stresses. The strain energy density W is assumed to depend only on second-order invariants of strains and strain gradients. The second-order invariant of strains is

$$\varepsilon_e = \sqrt{\frac{2}{3}\varepsilon_{\alpha\beta}\varepsilon_{\alpha\beta}}, \quad (5)$$

while there are three second-order invariants of strain gradients for an incompressible solid and they are given by [25]

$$\eta_{\alpha\alpha\gamma}\eta_{\beta\beta\gamma} \quad \eta_{\alpha\beta\gamma}\eta_{\alpha\beta\gamma} \quad \text{and} \quad \eta_{\alpha\beta\gamma}\eta_{\gamma\beta\alpha}. \quad (6)$$

Fleck and Hutchinson [4] combined the second invariants of strains and strain gradients to define a new effective strain as

$$E = \sqrt{\frac{2}{3}\varepsilon_{\alpha\beta}\varepsilon_{\alpha\beta} + c_1\eta_{\alpha\alpha\gamma}\eta_{\beta\beta\gamma} + c_2\eta_{\alpha\beta\gamma}\eta_{\alpha\beta\gamma} + c_3\eta_{\alpha\beta\gamma}\eta_{\gamma\beta\alpha}}, \quad (7)$$

where constants c_1 , c_2 and c_3 have the unit of square of length. Fleck and Hutchinson [4] proposed to determine these constants by fitting microscale experiments, as discussed in detail in Section 2.3. With the new effective strain E , the strain energy density takes the same form as that in uniaxial tension, i.e., for a power law material

$$W = \frac{n}{n+1}\Sigma_0 E_0 \left(\frac{E}{E_0}\right)^{n+1/n}, \quad (8)$$

where n is the plastic work hardening exponent, Σ_0 is the tensile yield stress, and E_0 is the yield strain ($= \Sigma_0/\text{Young's modulus}$). With Eqs. (7) and (8), the constitutive law (4) can then be written as

$$\sigma'_{\alpha\beta} = \frac{2}{3}\frac{\Sigma_0}{E_0} \left(\frac{E}{E_0}\right)^{\frac{1}{n}-1} \varepsilon_{\alpha\beta}, \quad (9)$$

$$\begin{aligned} \tau'_{\alpha\beta\gamma} = \frac{\Sigma_0}{E_0} \left(\frac{E}{E_0}\right)^{\frac{1}{n}-1} & \left[c_1\eta_{\delta\delta\gamma}\delta_{\alpha\beta} + c_2\eta_{\alpha\beta\gamma} + \frac{c_3}{2}(\eta_{\gamma\beta\alpha} + \eta_{\gamma\alpha\beta}) - \frac{1}{4}\left(c_1 + \frac{c_3}{2}\right)\eta_{\delta\delta\alpha}\delta_{\beta\gamma} \right. \\ & \left. - \frac{1}{4}\left(c_1 + \frac{c_3}{2}\right)\eta_{\delta\delta\beta}\delta_{\alpha\gamma} \right]. \end{aligned} \quad (10)$$

Here we emphasize that $\sigma'_{\alpha\beta}$ and $\tau'_{\alpha\beta\gamma}$ are symmetric and deviatoric, i.e., $\sigma'_{\alpha\beta} = \sigma'_{\beta\alpha}$, $\sigma'_{\alpha\alpha} = 0$, $\tau'_{\alpha\beta\gamma} = \tau'_{\beta\alpha\gamma}$ and $\tau'_{\alpha\gamma\gamma} = 0$.

Equilibrium equations in the higher-order continuum theory are

$$\sigma'_{\beta\alpha, \beta} - \tau'_{\beta\gamma\alpha, \beta\gamma} + H_{, \alpha} = 0, \quad \alpha = 1, 2, \quad (11)$$

where

$$H = \frac{1}{3}(\sigma_{\delta\delta} + \sigma_{33}) - \frac{1}{2}(\tau_{\alpha\gamma\gamma, \alpha} + \tau_{\alpha 33, \alpha} + \tau_{3\gamma\gamma, 3} + \tau_{333, 3}) \quad (12)$$

is a combined measure of hydrostatic stress and hydrostatic higher-order stress for incompressible solids.

For a semi-infinite crack coinciding with the negative x_1 axis, the traction-free conditions on the crack faces ($x_1 < 0, x_2 = 0$) in an incompressible solid can be written as

$$\hat{t}_1 = \sigma'_{21} - 2\tau'_{211,1} - \tau'_{221,2} + \tau'_{222,1} = 0, \tag{13a}$$

$$\hat{t}_2 = \sigma'_{22} - 2\tau'_{212,1} - \tau'_{222,2} + H = 0, \tag{13b}$$

$$\hat{r}_1 = \tau'_{221} = 0, \tag{13c}$$

where \hat{t}_1, \hat{t}_2 and \hat{r}_1 are the stress tractions and higher-order stress traction in the corresponding directions, respectively, and the unit normal on the crack face has been taken as $\mathbf{n} = (0, 1)$.

2.2. *J*-integral in strain gradient plasticity

The path-independent *J*-integral for classical plasticity [26] can be generalized for strain gradient plasticity as

$$J = \int_{\Gamma} \left[Wn_1 - (\hat{t}_k + Hn_k)u_{k,1} - \hat{r}_k Du_{k,1} \right] ds, \tag{14}$$

where Γ is an arbitrary contour surrounding the crack tip, originating from the lower crack face and ending at the upper crack face; n_k is the unit normal of the contour, W is the strain energy density in Eq. (8), H is the combined measure of hydrostatic stress and hydrostatic higher-order stress in Eq. (12), u_k is the displacement, and \hat{t}_k and \hat{r}_k are reduced stress tractions and higher-order stress tractions given by

$$\begin{aligned} \hat{t}_k + Hn_k &= n_i \left(\sigma'_{ik} - \tau'_{ijk,j} \right) + D_k \left(n_i n_j n_p \tau'_{ijp} \right) - D_j \left(n_i \tau'_{ijk} \right) + \left(n_i n_j \tau'_{ijk} - n_k n_i n_j n_p \tau'_{ijp} \right) \\ &\quad \times \left(D_q n_q \right) + Hn_k, \end{aligned} \tag{15}$$

$$\hat{r}_k = n_i n_j \tau'_{ijk} - n_k n_i n_j n_p \tau'_{ijp}. \tag{16}$$

The operators D and D_j in Eqs. (14) and (15) are the normal-gradient operator and surface-gradient operator, respectively, and are defined as

$$D \equiv n_k \frac{\partial}{\partial x_k}, \quad D_j \equiv \left(\delta_{jk} - n_j n_k \right) \frac{\partial}{\partial x_k}. \tag{17}$$

It is convenient to use the asymptotic crack tip field to evaluate the *J*-integral. In polar coordinates (r, θ) centered at the crack tip, the contour Γ can be taken as a circle of radius r such that the unit normal \mathbf{n} becomes the unit vector \mathbf{e}_r in the radial direction. The normal-gradient operator in Eq. (17) becomes $D = \frac{\partial}{\partial r}$. The tractions in Eqs. (15) and (16) are given by

$$\hat{\mathbf{t}} + H\mathbf{n} = \left(H - \frac{\partial \tau'_{rrr}}{\partial r} - \frac{2}{r} \frac{\partial \tau'_{r\theta r}}{\partial \theta} - \frac{2\tau'_{rrr} - 2\tau'_{r\theta\theta} - \tau'_{\theta\theta r}}{r} \right) \mathbf{e}_r + \left[-\frac{\partial \tau'_{rr\theta}}{\partial r} - \frac{1}{r} \frac{\partial}{\partial \theta} (2\tau'_{r\theta\theta} - \tau'_{rrr}) - \frac{\tau'_{rr\theta} + 2\tau'_{r\theta r} - \tau'_{\theta\theta\theta}}{r} \right] \mathbf{e}_\theta, \quad (18)$$

$$\hat{\mathbf{r}} = \tau'_{rr\theta} \mathbf{e}_\theta \quad (19)$$

where \mathbf{e}_θ is the unit vector in the circumferential direction θ .

2.3. Length scales in strain gradient plasticity

One important aspect of strain gradient plasticity is the length scale. From microscopic or dislocation point of view, this characteristic length has been identified as L_d^2/b [27], where L_d is the average spacing between dislocations and b is the Burger's vector. In terms of macroscopic shear modulus μ and uniaxial tensile yield stress σ_Y , this intrinsic material length is on the order of $(\frac{\mu}{\sigma_Y})^2 b$. From continuum mechanics point of view, however, this length scale is related to constants c_1 , c_2 and c_3 scaling the invariants of strain gradients, as discussed in the following.

Smyshlyaev and Fleck [25] have shown the strain gradient tensor η_{ijk} can be decomposed to a stretch gradient tensor, $\eta_{ijk}^{(1)}$, and two rotation gradient tensors, $\eta_{ijk}^{(2)}$ and $\eta_{ijk}^{(3)}$. The second invariants of strain gradients in Eq. (7) are related to these stretch and rotation gradients of deformation by

$$c_1 \eta_{\alpha\alpha\gamma} \eta_{\beta\beta\gamma} + c_2 \eta_{\alpha\beta\gamma} \eta_{\alpha\beta\gamma} + c_3 \eta_{\alpha\beta\gamma} \eta_{\gamma\beta\alpha} = l_1^2 \eta_{ijk}^{(1)} \eta_{ijk}^{(1)} + l_2^2 \eta_{ijk}^{(2)} \eta_{ijk}^{(2)} + l_3^2 \eta_{ijk}^{(3)} \eta_{ijk}^{(3)}, \quad (20)$$

where l_1 is the material length associated with the stretch gradients of deformation, while l_2 and l_3 are material lengths associated with rotational gradients of deformation. These lengths are related to constants c_1 , c_2 and c_3 by [4,25]

$$l_1^2 = c_2 + c_3, \quad l_2^2 = c_2 - \frac{c_3}{2}, \quad l_3^2 = \frac{5}{2}c_1 + c_2 - \frac{c_3}{4}. \quad (21)$$

From solutions to a variety of problems, it appears that only two of the three constitutive length parameters need to be treated as independent. The connection $l_3 = \sqrt{5/6}l_2$ will be enforced in the study which follows. By fitting micro-bend [14], micro-torsion [5], and micro-indentation data [8–13], Begley and Hutchinson [28] determined that l_1 , l_2 and l_3 scale with one material length, l ,

$$l_1 = \frac{l}{16} - \frac{l}{8}, \quad l_2 = \frac{l}{2}, \quad l_3 = \sqrt{\frac{5}{24}}l. \quad (22)$$

Their values for copper are $l \approx 4 \mu\text{m}$ with $l_1 \approx 0.25\text{--}0.5$, $l_2 \approx 2$ and $l_3 \approx 1.8 \mu\text{m}$, while the values for nickel are $l \approx 6 \mu\text{m}$ with $l_1 \approx 0.38\text{--}0.75$, $l_2 \approx 3$ and $l_3 \approx 2.7 \mu\text{m}$.

The rotation-gradient-based strain gradient plasticity theory [3,5] corresponds to the following choice of material length,

$$l_1 = 0, \quad l_2 = \frac{1}{2}, \quad l_3 = \sqrt{\frac{5}{24}}l. \tag{23}$$

This choice of material lengths, however, can predict only 10–20% increase of hardness in micro-indentation [29], which clearly falls short to agree with the 200–300% increase observed in experiments [8–13].

Gao et al. [6] and Huang et al. [7] developed dislocation models to connect the effective strain gradient with the density of geometrically necessary dislocations. They established the following choice of material lengths from dislocation models,

$$l_1 = l_2 = l_3 = \frac{1}{2}. \tag{24}$$

It is clear that l_2 and l_3 are quite close to those in Eq. (22), but l_1 is much larger for calibration against the dislocation models. This combination of material lengths gives the constants $c_1 = c_3 = 0$ and $c_2 = l^2/4$. Besides the differences in material lengths, Gao et al's [6] and Huang et al's [7] constitutive models are also different from those of phenomenological strain gradient plasticity [4]. However, the present study is limited to phenomenological strain gradient plasticity.

3. The asymptotic fields near a crack tip in strain gradient plasticity

Polar coordinates (r, θ) centered at the crack tip are used in the near-tip asymptotic analysis in this section, where crack faces coincide with $\theta = \pm\pi$. A displacement potential ϕ is introduced from the incompressibility of the crack tip field,

$$u_r = -\frac{1}{r} \frac{\partial \phi}{\partial \theta}, \quad u_\theta = \frac{\partial \phi}{\partial r}. \tag{25}$$

Similar to the HRR field [30,31] in classical plasticity, we look for a separable crack tip field, i.e., the displacement potential can be written as

$$\phi = r^{p+1} \tilde{\phi}(\theta), \tag{26}$$

where the power p ($p > 0$) and angular distribution $\tilde{\phi}(\theta)$ are to be determined. The displacements are obtained from Eq. (25) as

$$u_r = -r^p \tilde{\phi}'(\theta), \quad u_\theta = (p + 1)r^p \tilde{\phi}(\theta). \tag{27}$$

From kinematic relations (1) and (2), strains and strain gradients are given by

$$\varepsilon_{rr} = \frac{\partial u_r}{\partial r} = -pr^{p-1} \tilde{\phi}', \tag{28a}$$

$$\varepsilon_{\theta\theta} = \frac{1}{r} \frac{\partial u_\theta}{\partial \theta} + \frac{u_r}{r} = pr^{p-1} \tilde{\phi}', \tag{28b}$$

$$\varepsilon_{r\theta} = \varepsilon_{\theta r} = \frac{1}{2} \left(\frac{1}{r} \frac{\partial u_r}{\partial \theta} + \frac{\partial u_\theta}{\partial r} - \frac{u_\theta}{r} \right) = \frac{1}{2} r^{p-1} \left[-\tilde{\phi}'' + (p^2 - 1)\tilde{\phi} \right], \quad (28c)$$

$$\eta_{rrr} = \frac{\partial^2 u_r}{\partial r^2} = -p(p-1)r^{p-2}\tilde{\phi}', \quad (29a)$$

$$\eta_{rr\theta} = \frac{\partial^2 u_\theta}{\partial r^2} = p(p^2 - 1)r^{p-2}\tilde{\phi}, \quad (29b)$$

$$\eta_{r\theta r} = \eta_{\theta r r} = \frac{\partial}{\partial r} \left[\frac{1}{r} \left(\frac{\partial u_r}{\partial \theta} - u_\theta \right) \right] = -(p-1)r^{p-2} \left[\tilde{\phi}'' + (p+1)\tilde{\phi} \right], \quad (29c)$$

$$\eta_{r\theta\theta} = \eta_{\theta r\theta} = \frac{\partial}{\partial r} \left[\frac{1}{r} \left(\frac{\partial u_\theta}{\partial \theta} + u_r \right) \right] = p(p-1)r^{p-2}\tilde{\phi}', \quad (29d)$$

$$\eta_{\theta\theta r} = \frac{\partial}{\partial r} \left(\frac{u_r}{r} \right) + \frac{1}{r^2} \frac{\partial^2 u_r}{\partial \theta^2} - \frac{2}{r^2} \frac{\partial u_\theta}{\partial \theta} = -r^{p-2} \left[\tilde{\phi}''' + (3p+1)\tilde{\phi}' \right], \quad (29e)$$

$$\eta_{\theta\theta\theta} = \frac{\partial}{\partial r} \left(\frac{u_\theta}{r} \right) + \frac{1}{r^2} \frac{\partial^2 u_\theta}{\partial \theta^2} + \frac{2}{r^2} \frac{\partial u_r}{\partial \theta} = (p-1)r^{p-2} \left[\tilde{\phi}'' + (p+1)\tilde{\phi} \right]. \quad (29f)$$

They can generally be written as $\varepsilon_{\alpha\beta} = r^{p-1}\tilde{\varepsilon}_{\alpha\beta}(\theta)$ and $\eta_{\alpha\beta\gamma} = r^{p-2}\tilde{\eta}_{\alpha\beta\gamma}(\theta)$, where $\tilde{\varepsilon}_{\alpha\beta}$ and $\tilde{\eta}_{\alpha\beta\gamma}$ are angular distributions in Eqs. (28) and (29). Since strain gradients are more singular than strains near a crack tip, the dominant singular term in the effective strain in Eq. (7) can be written as

$$E = r^{p-2}\tilde{E}(\theta), \quad (30)$$

where

$$\tilde{E} = \sqrt{c_1\tilde{\eta}_{\alpha\alpha\gamma}\tilde{\eta}_{\beta\beta\gamma} + c_2\tilde{\eta}_{\alpha\beta\gamma}\tilde{\eta}_{\alpha\beta\gamma} + c_3\tilde{\eta}_{\alpha\beta\gamma}\tilde{\eta}_{\gamma\beta\alpha}}. \quad (31)$$

The constitutive relations (9) and (10) give the deviatoric stresses and deviatoric higher-order stresses as

$$\sigma'_{\alpha\beta} = \frac{\Sigma_0}{E_0^{1/n}} r^{\frac{p-2}{n}+1} \tilde{\sigma}'_{\alpha\beta}(\theta), \quad (32)$$

$$\tau'_{\alpha\beta\gamma} = \frac{\Sigma_0}{E_0^{1/n}} r^{\frac{p-2}{n}} \tilde{\tau}'_{\alpha\beta\gamma}(\theta), \quad (33)$$

where the angular distributions of stresses and higher-order stresses are related to the angular distributions of strains and strain gradients by

$$\tilde{\sigma}'_{\alpha\beta} = \frac{2}{3} \tilde{E}^{n-1} \tilde{\varepsilon}_{\alpha\beta}, \tag{34}$$

$$\begin{aligned} \tilde{\tau}'_{\alpha\beta\gamma} = \tilde{E}^{\frac{1-n}{n}} \left\{ c_1 \tilde{\eta}_{\delta\delta\gamma} \delta_{\alpha\beta} + c_2 \tilde{\eta}_{\alpha\beta\gamma} + \frac{c_3}{2} (\tilde{\eta}_{\gamma\beta\alpha} + \tilde{\eta}_{\gamma\alpha\beta}) - \frac{1}{4} \left(c_1 + \frac{c_3}{2} \right) \tilde{\eta}_{\delta\delta\alpha} \delta_{\beta\gamma} \right. \\ \left. - \frac{1}{4} \left(c_1 + \frac{c_3}{2} \right) \tilde{\eta}_{\delta\delta\beta} \delta_{\alpha\gamma} \right\}. \end{aligned} \tag{35}$$

The dominant singular term in the combined measure H of hydrostatic stress and hydrostatic higher-order stress in the crack tip field can be written as

$$H = \frac{\Sigma_0}{E_0^{1/n}} r^{\frac{p-2}{n}-1} \tilde{H}(\theta), \tag{36}$$

where \tilde{H} is the angular distribution of H and is to be determined.

In polar coordinates (r, θ) , the equilibrium equations (11) take the following form,

$$\frac{\partial \sigma_{rr}^*}{\partial r} + \frac{1}{r} \frac{\partial \sigma_{\theta r}^*}{\partial \theta} + \frac{\sigma_{rr}^* - \sigma_{\theta\theta}^*}{r} = 0, \tag{37a}$$

$$\frac{\partial \sigma_{r\theta}^*}{\partial r} + \frac{1}{r} \frac{\partial \sigma_{\theta\theta}^*}{\partial \theta} + \frac{\sigma_{r\theta}^* + \sigma_{\theta r}^*}{r} = 0, \tag{37b}$$

where

$$\sigma_{rr}^* = \sigma'_{rr} + H - \left(\frac{\partial \tau'_{rrr}}{\partial r} + \frac{1}{r} \frac{\partial \tau'_{\theta rr}}{\partial \theta} + \frac{\tau'_{rrr} - \tau'_{\theta r\theta} - \tau'_{\theta\theta r}}{r} \right), \tag{38a}$$

$$\sigma_{\theta r}^* = \sigma'_{\theta r} - \left(\frac{\partial \tau'_{r\theta r}}{\partial r} + \frac{1}{r} \frac{\partial \tau'_{\theta\theta r}}{\partial \theta} + \frac{\tau'_{r\theta r} + \tau'_{\theta rr} - \tau'_{\theta\theta\theta}}{r} \right), \tag{38b}$$

$$\sigma_{r\theta}^* = \sigma'_{r\theta} - \left(\frac{\partial \tau'_{rr\theta}}{\partial r} + \frac{1}{r} \frac{\partial \tau'_{\theta r\theta}}{\partial \theta} + \frac{\tau'_{rr\theta} + \tau'_{\theta rr} - \tau'_{\theta\theta\theta}}{r} \right), \tag{38c}$$

$$\sigma_{\theta\theta}^* = \sigma'_{\theta\theta} + H - \left(\frac{\partial \tau'_{r\theta\theta}}{\partial r} + \frac{1}{r} \frac{\partial \tau'_{\theta\theta\theta}}{\partial \theta} + \frac{\tau'_{r\theta\theta} + \tau'_{\theta r\theta} + \tau'_{\theta\theta r}}{r} \right). \tag{38d}$$

Since the deviatoric stresses are less singular than the higher-order deviatoric stresses and hydrostatic stress H , they are negligible in the asymptotic crack tip field. The substitution of the asymptotic expressions (33) and (36) into the equilibrium equations (37) gives

$$\begin{aligned} \frac{d^2 \tilde{\tau}'_{\theta\theta r}}{d\theta^2} + 2\left(\frac{p-2}{n} + 1\right) \frac{d\tilde{\tau}'_{\theta rr}}{d\theta} - 2\frac{d\tilde{\tau}'_{\theta\theta\theta}}{d\theta} + \left(\frac{p-2}{n} + 1\right) \frac{p-2}{n} \tilde{\tau}'_{rrr} - 2\left(\frac{p-2}{n} + 1\right) \tilde{\tau}'_{r\theta\theta} \\ - \left(\frac{p-2}{n} + 1\right) \tilde{\tau}'_{\theta\theta r} - \left(\frac{p-2}{n} - 1\right) \tilde{H} = 0, \end{aligned} \quad (39a)$$

$$\begin{aligned} \frac{d^2 \tilde{\tau}'_{\theta\theta\theta}}{d\theta^2} + 2\left(\frac{p-2}{n} + 1\right) \frac{d\tilde{\tau}'_{r\theta\theta}}{d\theta} + 2\frac{d\tilde{\tau}'_{\theta\theta r}}{d\theta} + \left(\frac{p-2}{n} + 1\right) \frac{p-2}{n} \tilde{\tau}'_{rr\theta} \\ + 2\left(\frac{p-2}{n} + 1\right) \tilde{\tau}'_{\theta rr} - \left(\frac{p-2}{n} + 1\right) \tilde{\tau}'_{\theta\theta\theta} - \frac{d\tilde{H}}{d\theta} = 0, \end{aligned} \quad (39b)$$

where the symmetry $\tau'_{r\theta r} = \tau'_{\theta r r}$, $\tau'_{\theta r\theta} = \tau'_{r\theta\theta}$ has been used. The replacement of $\tilde{\tau}'_{\alpha\beta\gamma}$ in the above equations by the angular function $\tilde{\phi}$ of the displacement potential via Eq. (35) yields two ordinary differential equations for $\tilde{\phi}$ and \tilde{H} .

In polar coordinates (r, θ) , the traction-free boundary conditions (13) can be written as

$$-2\frac{\partial \tau'_{\theta rr}}{\partial r} - \frac{1}{r} \frac{\partial \tau'_{\theta\theta r}}{\partial \theta} - \frac{2\tau'_{\theta rr} - \tau'_{\theta\theta\theta}}{r} + \frac{\partial \tau'_{\theta\theta\theta}}{\partial r} = 0 \quad \text{at } \theta = \pi, \quad (40a)$$

$$-2\frac{\partial \tau'_{r\theta\theta}}{\partial r} - \frac{1}{r} \frac{\partial \tau'_{\theta\theta\theta}}{\partial \theta} - \frac{2\tau'_{r\theta\theta} + \tau'_{\theta\theta r}}{r} + H = 0 \quad \text{at } \theta = \pi, \quad (40b)$$

$$\tau'_{\theta\theta r} = 0 \quad \text{at } \theta = \pi, \quad (40c)$$

where deviatoric stresses in Eq. (13) have been neglected since they are less singular. The substitution of asymptotic expressions (9) and (12) into the above boundary conditions gives

$$\frac{d\tilde{\tau}'_{\theta\theta r}}{d\theta} + 2\left(\frac{p-2}{n} + 1\right) \tilde{\tau}'_{\theta rr} - \left(\frac{p-2}{n} + 1\right) \tilde{\tau}'_{\theta\theta\theta} = 0 \quad \text{at } \theta = \pi, \quad (41a)$$

$$\frac{d\tilde{\tau}'_{\theta\theta\theta}}{d\theta} + 2\left(\frac{p-2}{n} + 1\right) \tilde{\tau}'_{r\theta\theta} + \tilde{\tau}'_{\theta\theta r} - \tilde{H} = 0 \quad \text{at } \theta = \pi, \quad (41b)$$

$$\tilde{\tau}'_{\theta\theta r} = 0 \quad \text{at } \theta = \pi. \quad (41c)$$

The symmetry condition ahead of a mode I crack tip ($\theta = 0$) requires $\tilde{\phi}$ be an odd function of θ such that

$$\tilde{\phi} = \tilde{\phi}^{(2)} = \tilde{\phi}^{(4)} = 0 \quad \text{at } \theta = 0, \quad (42)$$

or equivalently,

$$\eta_{rr\theta} = \eta_{\theta\theta\theta} = \frac{\partial \eta_{\theta\theta r}}{\partial \theta} = 0 \quad \text{at } \theta = 0. \quad (43)$$

Eqs. (39), boundary conditions (41) and (42) constitute an eigenvalue problem for mode I crack tip fields in strain gradient plasticity, with the power p as the eigenvalue and $\tilde{\phi}$ and \tilde{H} as the eigenvector. However, due to the path-independent J -integral (14) in strain gradient plasticity, it can be shown that the strain energy density is of the order of r^{-1} , such that the power p is known a priori as,

$$p = \frac{n+2}{n+1}, \quad (44)$$

where $n (> 1)$ is the plastic work hardening exponent.

Similar to the HRR field in classical plasticity [30,31], a numerical shooting method is used to solve the ordinary differential equations (39), (41) and (42). Details of the numerical method are given in the Appendix A. Only the asymptotic crack tip fields are presented in the following.

In all studies, the plastic work hardening exponent n is fixed at a typical value of $n = 5$, while three combinations of the material lengths l_1 , l_2 and l_3 are given by,

$$l_1 = 0, \quad l_2 = \frac{l}{2}, \quad l_3 = \sqrt{\frac{5}{24}}l, \quad (45)$$

$$l_1 = \frac{l}{16} - \frac{l}{8}, \quad l_2 = \frac{l}{2}, \quad l_3 = \sqrt{\frac{5}{24}}l, \quad (46)$$

$$l_1 = l_2 = l_3 = \frac{l}{2}, \quad (47)$$

where l is an intrinsic material length. These combinations of material lengths correspond respectively to rotation-gradient-based strain gradient plasticity [3,5], phenomenological strain gradient plasticity theory [4] which accounts for both rotation and stretch gradients of deformation, and the dislocation models to connect strain gradient plasticity with the density of geometrically necessary dislocations [6,7].

3.1. Rotation-gradient-based strain gradient plasticity ($l_1=0$, $l_2=\frac{l}{2}$, $l_3=\sqrt{\frac{5}{24}}l$)

Huang et al. [18] and Xia and Hutchinson [20] obtained analytically the asymptotic fields near a mode I crack tip in rotation-gradient-based strain gradient plasticity. They established that the crack tip deformation field is irrotational such that the strains and stresses are more singular than curvatures (strain gradients) and higher-order stresses, respectively. The corresponding power p for displacements in this stress-dominated (stresses are more singular than higher-order stresses) crack tip field is $p = 1/(n+1)$, which is the same as the HRR field [30,31] in classical plasticity (even though the two asymptotic fields are different). Moreover, besides the stress-dominated crack tip field, Huang et al. [18] established that there is another mode I crack tip field in which the higher-order stresses are more singular than stresses, i.e., the higher-order-stress-dominated crack tip field. This field is clearly rotational since the rotation gradients of deformation become the dominating singular terms. The corresponding

power p for displacements in the higher-order-stress-dominated crack tip field is $p = (n + 2)/(n + 1)$.

For the power $p = 1/(n + 1)$ and material lengths $l_1 = 0$, $l_2 = \frac{1}{2}$ and $l_3 = \sqrt{\frac{5}{24}}l$, our numerical shooting method gives a single solution that is identical to the analytic stress-dominated crack tip field of Huang et al. [18] and Xia and Hutchinson [20]. For the power $p = (n + 2)/(n + 1)$, our numerical shooting method gives another solution that is identical to the analytic higher-order-stress-dominated crack tip field obtained by Huang et al. [18]. The agreement between analytical and numerical studies provides a validation of the numerical method given in the Appendix A.

3.2. Phenomenological strain gradient plasticity ($l_1 = \frac{1}{16} - \frac{1}{8}$, $l_2 = \frac{1}{2}$, $l_3 = \sqrt{\frac{5}{24}}l$)

The phenomenological strain gradient plasticity theory [4] includes both stretch gradients and rotation gradients of deformation. Because of the stretch gradients, strain gradients and higher-order stresses in the asymptotic crack tip field are more singular than strains and stresses, respectively. Therefore, the dominant singular term in the effective strain is given by

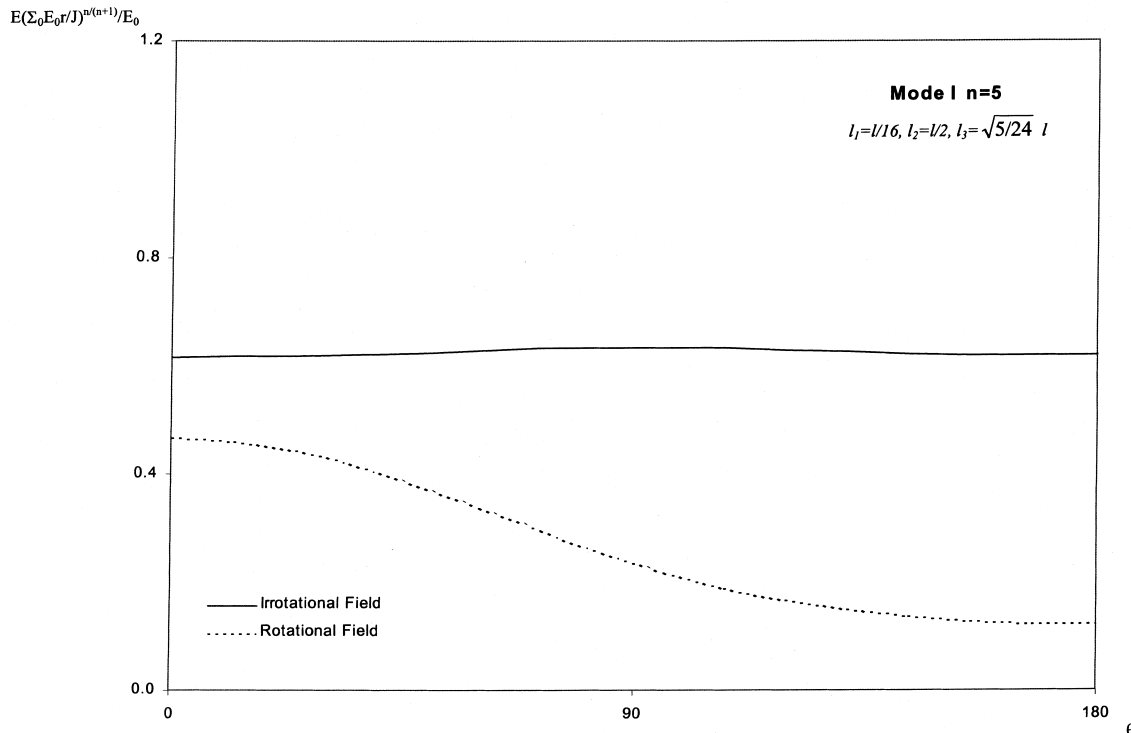


Fig. 1. Angular distributions of normalized effective strain $E(\Sigma_0 E_0 r/J)^{n/(n+1)}/E_0$ for two mode I crack tip fields in phenomenological strain gradient plasticity; Σ_0 is the tensile yield stress, E_0 is the yield strain ($= \Sigma_0/\text{Young's modulus}$), r is the distance to the crack tip, J is the J -integral, $n = 5$ is the plastic work hardening exponent, and the combination of material lengths is $l_1 = l/16$, $l_2 = l/2$, $l_3 = \sqrt{5/24}l$.

Eq. (30), and the power p of the displacements in the crack tip field is given by Eq. (44), i.e., $p = (n + 2)/(n + 1)$.

For each material length l_1 between $\frac{1}{16}$ and $\frac{1}{8}$, the numerical shooting method gives two solutions, i.e., there are two different mode I crack tip fields for the same material, which is quite puzzling. We examine the limit $l_1 = 0$ in order to understand the structure of mode I crack tip field in strain gradient plasticity. As l_1 decreases and approaches zero, numerical solutions show that the difference between two crack tip fields shrinks and both fields approach Huang et al. [18] analytic higher-order-stress-dominated crack tip field in rotation-gradient-based strain gradient plasticity. Similar to an eigen problem with two identical eigenvalues, the second independent solution at the limit $l_1 = 0$ turns out to be the stress-dominated crack tip field [18,20], i.e., there are also two independent solutions at the limit $l_1 = 0$.

The crack faces should have an opening displacement in mode I fracture. This requires $u_\theta (\theta = \pi) < 0$, which uniquely determines the sign of the solution in an eigenvalue problem.

The angular distributions of the effective strain for the two crack tip fields are shown in Fig. 1 for material lengths $l_1 = \frac{1}{16}$, $l_2 = \frac{1}{2}$ and $l_3 = \sqrt{\frac{5}{24}}l$. It is observed that the effective strain for

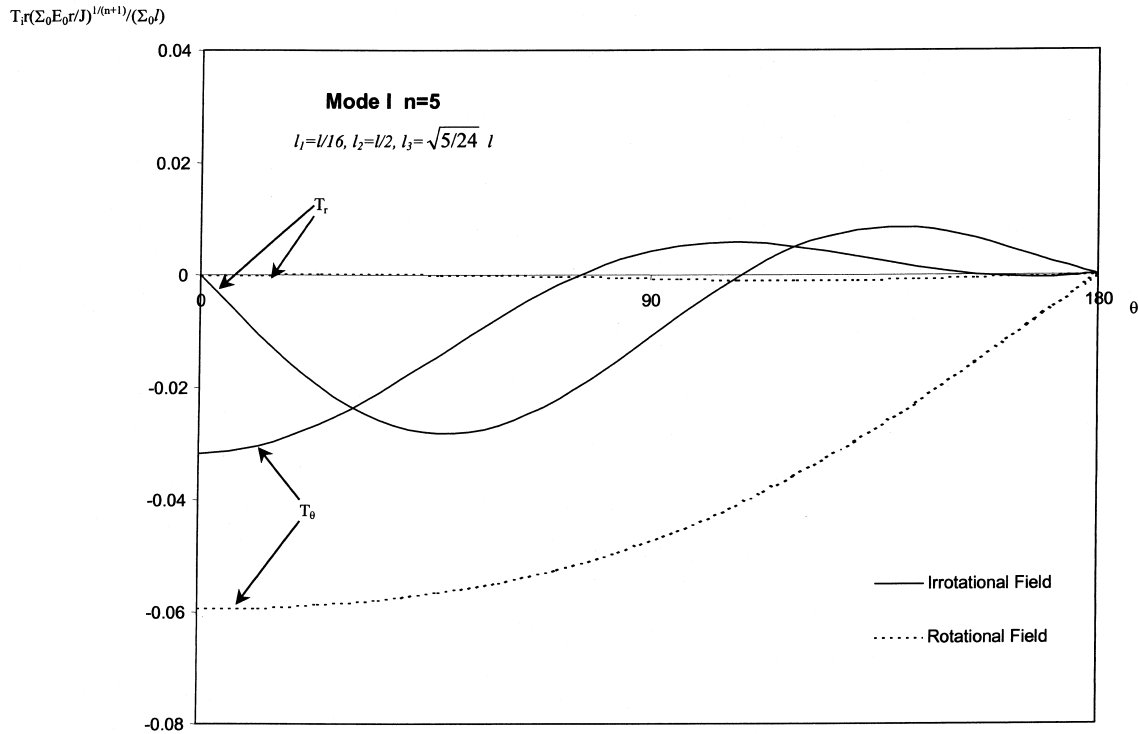


Fig. 2. Angular distributions of normalized reduced stress tractions $T_r r (\Sigma_0 E_0 r / J)^{1/(n+1)} / (\Sigma_0 l)$ and $T_\theta r (\Sigma_0 E_0 r / J)^{1/(n+1)} / (\Sigma_0 l)$ for two mode I crack tip fields in phenomenological strain gradient plasticity; T_r and T_θ are respectively the tractions in the radial and circumferential directions, on a ray through the crack tip ($\theta = \text{constant}$), the unit normal of the ray is taken as e_θ ; Σ_0 is the tensile yield stress, E_0 is the yield strain ($= \Sigma_0 / \text{Young's modulus}$), r is the distance to the crack tip, J is the J -integral, $n = 5$ is the plastic work hardening exponent, and the combination of material lengths is $l_1 = l/16$, $l_2 = l/2$, $l_3 = \sqrt{5/24}l$.

one crack tip field (solid line) is nearly independent of the polar angle θ . The numerical solution has verified that the rotation gradients of deformation for this field are two orders of magnitude smaller than the stretch gradients such that this crack tip field is nearly irrotational. The other curve (dotted line) in Fig. 1, however, shows a clear dependence on the polar angle θ . This field is rotational near a mode I crack tip in strain gradient plasticity because the magnitude of the rotational gradients of deformations is even larger than that of the stretch gradients. Accordingly, the two crack tip fields are denoted by “irrotational field” and “rotational field” in Fig. 1. The two crack tip fields have quite different angular distributions, and for the same J -integral, the irrotational field has a larger effective strain than the rotational field.

The angular distributions of reduced stress tractions T_r and T_θ in the irrotational and rotational crack tip fields are shown in Fig. 2 for material lengths $l_1 = \frac{l}{16}$, $l_2 = \frac{l}{2}$ and $l_3 = \sqrt{\frac{5}{24}}l$, where T_r and T_θ are respectively the tractions in the radial and circumferential directions, on a ray through the crack tip ($\theta = \text{constant}$). The unit normal of the ray is taken as e_θ , which is the unit vector in the circumferential direction. In polar coordinates (r, θ) , these tractions are given by

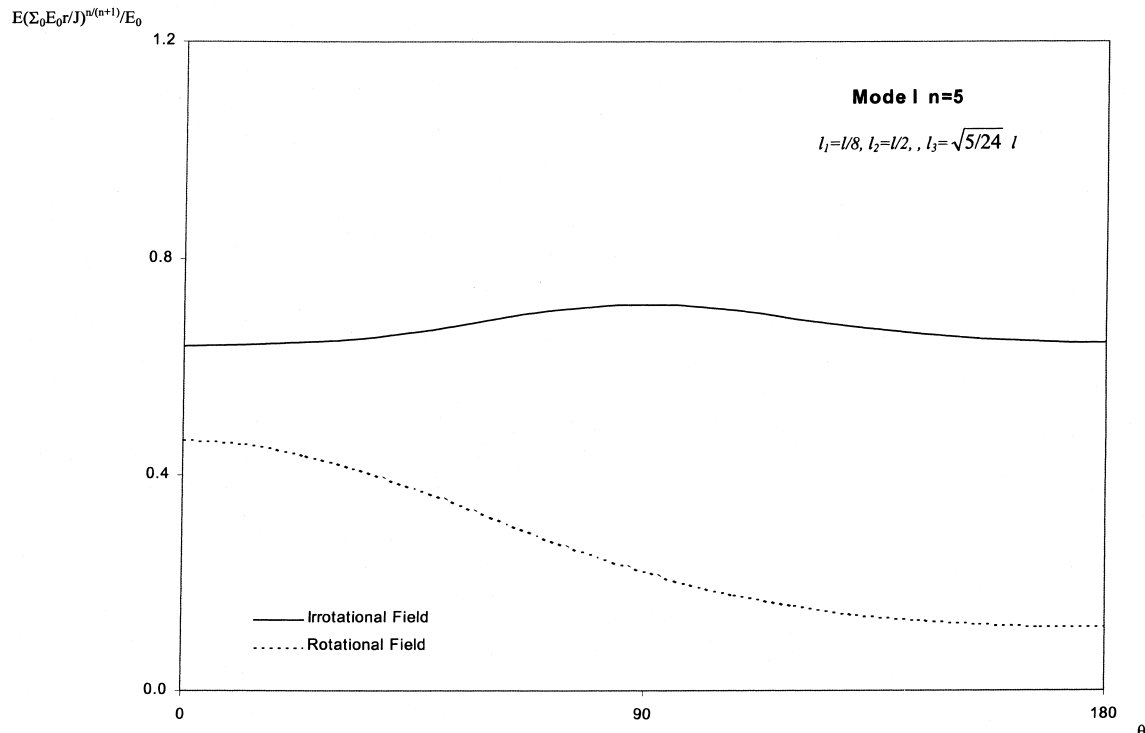


Fig. 3. Angular distributions of normalized effective strain $E(\Sigma_0 E_0 r/J)^{n/(n+1)}/E_0$ for two mode I crack tip field in phenomenological strain gradient plasticity; Σ_0 is the tensile yield stress, E_0 is the yield strain ($\Sigma_0 = \text{Young's modulus}$), r is the distance to the crack tip, J is the J -integral, $n = 5$ is the plastic work hardening exponent, and the combination of material lengths is $l_1 = l/8$, $l_2 = l/2$, $l_3 = \sqrt{5/24}l$.

$$T_r = -2 \frac{\partial \tau'_{\theta rr}}{\partial r} - \frac{1}{r} \frac{\partial \tau'_{\theta \theta r}}{\partial \theta} - \frac{2\tau'_{\theta rr} - \tau'_{\theta \theta \theta}}{r} + \frac{\partial \tau'_{\theta \theta \theta}}{\partial r}, \tag{48}$$

$$T_\theta = -2 \frac{\partial \tau'_{r\theta\theta}}{\partial r} - \frac{1}{r} \frac{\partial \tau'_{\theta\theta\theta}}{\partial \theta} - \frac{2\tau'_{r\theta\theta} + \tau'_{\theta\theta r}}{r} + H. \tag{49}$$

The stress tractions in the irrotational and rotational crack tip fields are quite different. For example, the shear stress traction T_r in the rotational field is nearly zero, while its counterpart in the irrotational field is significant and is of the same order as the normal stress traction T_θ . One important observation from Fig. 2 is that, for both irrotational and rotational fields, the normal traction component T_θ at $\theta = 0$ is compressive. (T_r and T_θ are evaluated on the plane $\theta = \text{constant}$ with the unit normal $\mathbf{n} = \mathbf{e}_\theta$, thus a negative T_θ implies a compressive normal traction.) This result is counterintuitive, suggesting that the asymptotic field lies outside the domain of physical validity. This is indeed the case as has been found from a full field numerical solution to the problem. Look ahead to this solution in Fig. 5, which will be introduced more completely in the next section, one sees that for the case of Poisson’s ratio

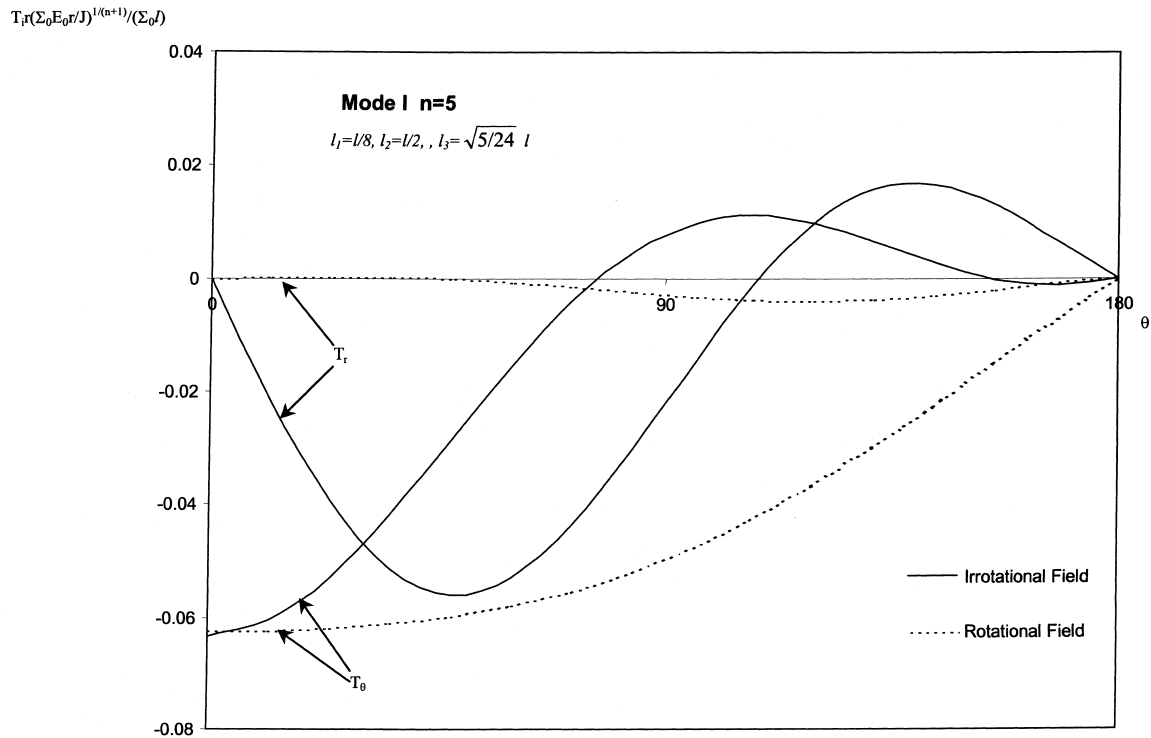


Fig. 4. Angular distributions of normalized reduced stress tractions $T_r r(\Sigma_0 E_0 r/J)^{1/(n+1)}/(\Sigma_0 l)$ and $T_\theta r(\Sigma_0 E_0 r/J)^{1/(n+1)}/(\Sigma_0 l)$ for two mode I crack tip fields in phenomenological strain gradient plasticity; T_r and T_θ are respectively the tractions in the radial and circumferential directions, on a ray through the crack tip ($\theta = \text{constant}$), the unit normal of the ray is taken as \mathbf{e}_θ ; Σ_0 is the tensile yield stress, E_0 is the yield strain ($= \Sigma_0/\text{Young's modulus}$), r is the distance to the crack tip, J is the J -integral, $n = 5$ is the plastic work hardening exponent, and the combination of material lengths is $l_1 = l/8, l_2 = l/2, l_3 = \sqrt{5/24}l$.

$\nu = 0.48$ and $\nu = 0.49$, the normal traction ahead of the tip becomes compressive only for $r/l < 0.05$. The tensile traction increases monotonically as the tip is approached until $r/l \approx 0.15$. The strain gradient plasticity theory is not expected to be valid at deformation scales which are much less than l . Thus, while the asymptotic field may have a tiny range of mathematical validity (i.e., $r/l \ll 0.05$), it has no range of physical validity.

Fig. 3 shows the angular distributions of the effective strain for the two crack tip fields and another combination of material lengths $l_1 = \frac{l}{8}$, $l_2 = \frac{l}{2}$ and $l_3 = \sqrt{\frac{5}{24}}l$. Similar to Fig. 1, the effective strain for one crack tip field (solid line) depends very weakly on the polar angle θ , and the corresponding field is named the nearly irrotational field. The other curve (dotted one) is denoted by the rotational field because of its clear dependence on the polar angle θ . The numerical solutions have verified that the rotation gradients of deformation are two orders of magnitude smaller than the stretch gradients in the nearly irrotational field, but become larger in the rotational field. Although the effective strains in the irrotational and rotational crack tip fields are quite different in Fig. 3, they are almost identical to the corresponding curves for $l_1 = \frac{l}{16}$ in Fig. 1, i.e., the effective strains are essentially independent of the material length l_1 in phenomenological strain gradient plasticity ($l_1 = \frac{l}{16} - \frac{l}{8}$).

The angular distributions of the reduced stress tractions T_r and T_θ are shown in Fig. 4 for both irrotational and rotational crack tip fields and the material lengths $l_1 = \frac{l}{8}$, $l_2 = \frac{l}{2}$ and $l_3 = \sqrt{\frac{5}{24}}l$. It is once again observed that the normal traction component T_θ at $\theta = 0$ is compressive. This is consistent with that in Fig. 2, and is contradictory again to the “correct” tensile stress at $\theta = 0$ in a mode I crack tip field. This confirms the conclusion that the mode I asymptotic crack tip field has no domain of physical validity in phenomenological strain gradient plasticity.

3.3. Dislocation models for strain gradient plasticity ($l_1 = l_2 = l_3 = \frac{l}{2}$)

The phenomenological strain gradient plasticity theory [4] with material lengths $l_1 = \frac{l}{16} \sim \frac{l}{8}$, $l_2 = \frac{l}{2}$ and $l_3 = \sqrt{\frac{5}{24}}l$ gives two solutions for the mode I crack tip fields. However, for material lengths $l_1 = l_2 = l_3 = l/2$, the numerical shooting method gives only a single solution for the mode I crack tip field (Fig. 7). We have verified that it is the material length l_1 scaling the stretch gradients that governs whether the crack tip field has one or two solutions. The mode I crack tip field for $l_1 = l_2 = l_3 = l/2$ is rotational since its angular distribution of the effective strain depends strongly on the polar angle θ . The corresponding normal traction component T_θ at $\theta = 0$ is also compressive, consistent with those in Figs. 2 and 4. This once again contradicts the tensile normal stress expected for a mode I crack tip field.

We have also studied the mode II crack tip fields in phenomenological strain gradient plasticity for all combinations of material lengths in Eqs. (45)–(47) (see [32] for details). The same conclusion has also been reached for mode II that the asymptotic crack tip fields have no domain of physical validity in phenomenological strain gradient plasticity. The asymptotic crack tip fields have the domain of mathematical validity of a tiny fraction of material length l , and strain gradient plasticity is not expected to be valid in this domain.

4. Finite element analysis for strain gradient plasticity

The finite element method for rotation-gradient-based strain gradient plasticity was developed by Xia and Hutchinson [20]. Several new elements were developed for the higher order theory, and were used to study fracture [20,22,23] and micro-indentation [29]. Begley and Hutchinson [28] generalized these elements to account for stretch gradients of deformation in the study of micro-indentation experiments. Since the crack tip deformation is nearly incompressible and stretch gradients are large, Wei and Hutchinson [33] developed a new finite element method using an element especially suited to the higher order theory. Details of this new finite element method will be published elsewhere. This element has been validated for the limit of plastic work hardening exponent $n = 1$, for which Shi et al. [34] have obtained the full-field solution analytically using the Wiener–Hopf method of analytic continuation. The numerical solution based on this new element agrees remarkably well with Shi et al. [34] analytic solution not only near the crack tip, but also throughout the entire field. This agreement shows that the new element developed by Wei and Hutchinson [33] can indeed capture the effects of both stretch and rotation gradients of deformation near a crack tip.

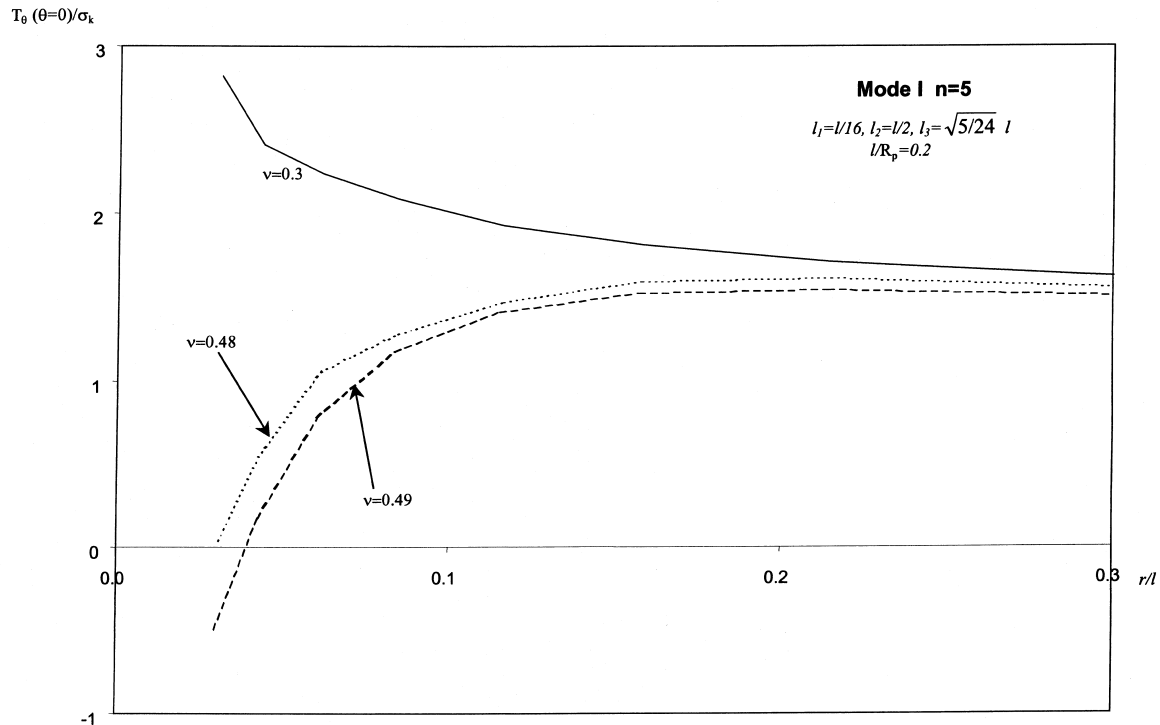


Fig. 5. Normalized normal traction T_0/σ_K along $\theta = 0$ versus the normalized distance r/l to a mode I crack tip in phenomenological strain gradient plasticity; the unit normal is taken as $e_\theta = (0,1)$; $\sigma_K = K_I/\sqrt{2\pi l}$, K_I is the remotely applied mode I stress intensity factor; l is the material length; $n = 5$ is the plastic work hardening exponent; the combination of material lengths is $l_1 = l/16$, $l_2 = l/2$, $l_3 = \sqrt{5/24}l$; the ratio of material length l to the plastic zone size R_p is $l/R_p = 0.2$; solutions are presented for Poisson's ratios $\nu = 0.3, 0.48$ and 0.49 .

We have used this new element to analyze the full field solution in phenomenological strain gradient plasticity [4] for the plastic work hardening exponent $n = 5$. The classical elastic K_I field is imposed as the remote boundary condition. Wei and Hutchinson [35] have identified a measure of remote loading in strain gradient plasticity as the ratio of intrinsic material length to the plastic zone size, l/R_p , where the plastic zone size R_p can be estimated as

$$R_p = \frac{K_I^2}{3\pi\Sigma_0^2}, \quad (50)$$

where K_I is the remotely applied stress intensity factor, and Σ_0 is the tensile yield stress. Figs. 5–7 show the normal stress traction T_θ at $\theta = 0$ versus the distance r to a mode I crack tip, where the unit normal is $\mathbf{n} = \mathbf{e}_\theta = (0, 1)$, and the normal stress traction T_θ is normalized by

$$\sigma_K = \frac{K_I}{\sqrt{2\pi l}}. \quad (51)$$

The material lengths in Figs. 5 and 6 are $l_1 = \frac{l}{16}$ and $l_1 = \frac{l}{8}$, respectively, with $l_2 = \frac{l}{2}$ and $l_3 =$

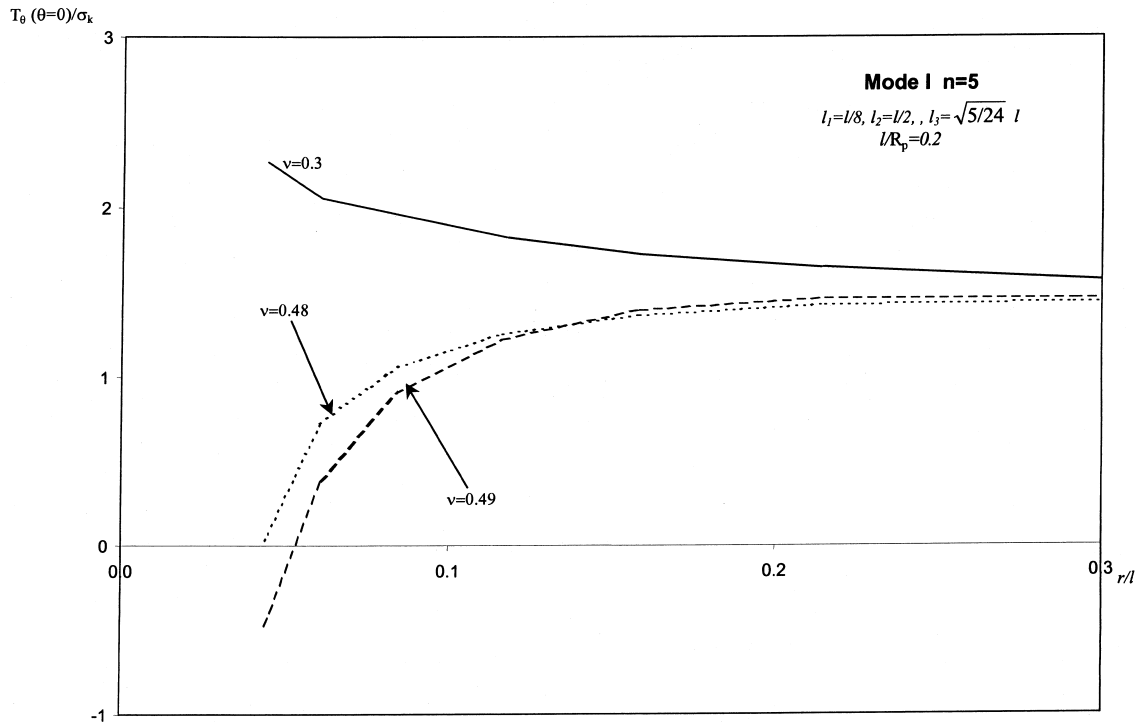


Fig. 6. Normalized normal traction T_θ/σ_K along $\theta = 0$ versus the normalized distance r/l to a mode I crack tip in phenomenological strain gradient plasticity; the unit normal is taken as $\mathbf{e}_\theta = (0,1)$; $\sigma_K = K_I/\sqrt{2\pi l}$, K_I is the remotely applied mode I stress intensity factor; l is the material length; $n = 5$ is the plastic work hardening exponent; the combination of material lengths is $l_1 = l/8$, $l_2 = l/2$, $l_3 = \sqrt{5/24}l$; the ratio of material length l to the plastic zone size R_p is $l/R_p = 0.2$; solutions are presented for Poisson's ratios $\nu = 0.3, 0.48$ and 0.49 .

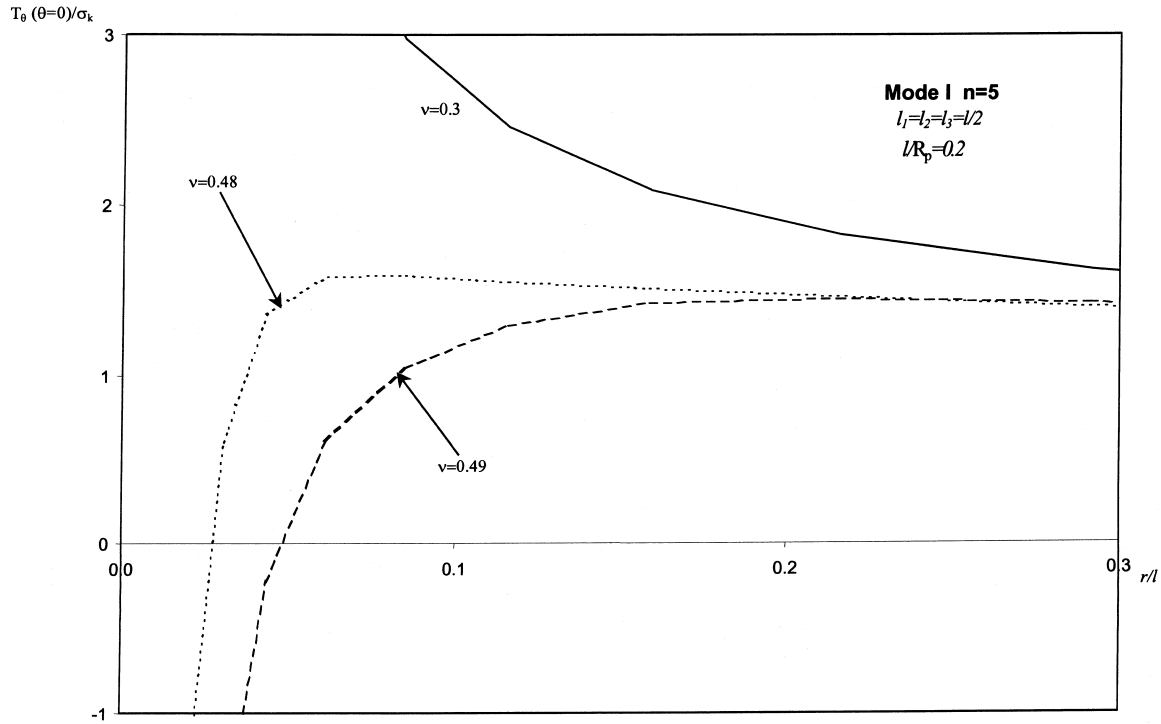


Fig. 7. Normalized normal traction T_θ/σ_K along $\theta = 0$ versus the normalized distance r/l to a mode I crack tip in phenomenological strain gradient plasticity; the unit normal is taken as $e_\theta = (0, 1)$; $\sigma_K = K_I/\sqrt{2\pi l}$, K_I is the remotely applied mode I stress intensity factor; l is the material length; $n = 5$ is the plastic work hardening exponent; the combination of material lengths is $l_1 = l_2 = l_3 = l/2$; the ratio of material length l to the plastic zone size R_p is $l/R_p = 0.2$; solutions are presented for Poisson's ratios $\nu = 0.3, 0.48$ and 0.49 .

$\sqrt{\frac{5}{24}}l$ as in Eq. (46), while Fig. 7 corresponds to $l_1 = l_2 = l_3 = \frac{l}{2}$ as in Eq. (47). The ratio of intrinsic material length l to plastic zone size R_p is $l/R_p = 0.2$. Three Poisson's ratios, $\nu = 0.30, 0.48$ and 0.49 , are taken in each figure, where the latter two are close to the limit for incompressible solids. For $\nu = 0.49$, it is observed that T_θ in Figs. 5–7 switch from a tensile stress to a compressive stress at a distance $r \approx 0.05l$ as the crack tip is approached. Therefore, within a distance of $0.05l$ to a mode I crack tip, the normal stress traction has the “incorrect” sign. However, well outside this domain, the normal stress traction ahead of the crack tip not only has the correct sign but also is significantly elevated due to strain gradient hardening. Similar observations are made for Poisson's ratio $\nu = 0.48$ in Figs. 5–7, but the curves for Poisson's ratio $\nu = 0.3$ are quite different; normal stress tractions remain to be tensile at the distance $r \approx 0.05l$ to the crack tip, and the curves continue to increase as the crack tip is approached. This seems to suggest that the incompressibility of solids may play a significant role in the asymptotic crack tip field. Further investigations would be necessary to resolve this. However, since the effect of incompressibility is limited to a domain outside the physical relevance of the constitutive theory, the justification for doing this would be questionable.

5. Discussion and conclusions

The asymptotic crack tip fields are obtained for mode I cracks in solids characterized by phenomenological strain gradient plasticity proposed by Fleck and Hutchinson [4]. In addition, the full-field solutions are also obtained by a finite element method using elements especially suited to the higher order theory. The following conclusions are established from the present analysis.

1. The asymptotic crack tip field provides a numerically accurate representation of the full-field solution only within a distance from the crack tip that is a tiny fraction of the constitutive length parameter l for strain gradient plasticity ($l \sim$ microns). The strain gradient plasticity theory is not expected to be valid in this domain.
2. The normal traction across the extended crack line ahead of the tip predicted by the asymptotic analysis is compressive. Therefore, the asymptotic field has no domain of physical validity.
3. The stress tractions are significantly elevated ahead of the crack tip due to strain gradient effects. The elevation occurs at distances from the crack tip which are well outside the tiny domain of validity of the asymptotic crack tip field, i.e., it occurs in a region where strain gradient plasticity theories are expected to be applicable.

There may be difficulties in understanding a compressive stress traction near a mode I crack tip in phenomenological strain gradient plasticity as well as its consequence of no domain of physical validity of the asymptotic crack tip field. It may be helpful to draw a loose analogy to the asymptotic field around an interface crack tip between two dissimilar elastic materials. It is well known that crack faces have contact near an interface crack tip (e.g., [36]). Even though this renders the asymptotic crack tip field inappropriate within a small distance from the tip, the fields hold well outside this contact zone. Similarly, even though the asymptotic crack tip field in phenomenological strain gradient plasticity has no domain of physical validity, strain gradient effects can significantly elevate the stress tractions ahead of a crack tip in a region where the strain gradient plasticity theories are expected to be applicable.

The loss of physical validity of the crack tip fields very near the tip does not necessarily invalidate the use of J as the measure of the crack loading intensity for stationary cracks. Again, the elastic bimaterial interface crack problem provides a useful analog. As long as there exists an annular region surrounding the tip wherein the strain gradient theory has physical validity, the J -integral characterizes the intensity passed down to the tip, even though the full solution very near the tip is not known. Recent efforts in simulation of fracture initiation and crack growth make use of an embedded cohesive zone characterized by a work of separation and a separation strength. If the length of the cohesive zone is not very small compared to the constitutive length parameter, the issue of the behavior of the asymptotic solution is moot.

Acknowledgements

The work of Y.H. was supported by the NSF through grants CMS-98-96285, Ford Foundation, and NSF of China. The work of J.W.H. was supported in part by the ONR

through grant N00014-96-10059 and by the NSF through grant CMS-96-34632. The work of K.C.H. was supported by NSF of China.

Appendix A. The numerical method

Eqs. (39) are the sixth-order ordinary differential equations (fifth order with respect to $\tilde{\phi}$ and first order with respect to \tilde{H}). Three boundary conditions are given in Eqs. (41) on the crack face ($\theta = \pi$), while the other three are the symmetry conditions (42) for mode I at $\theta = 0$. Therefore, a numerical shooting method [37] is used to solve the ordinary differential equations.

It is convenient to write the sixth-order ordinary differential equations for $\tilde{\phi}$ and \tilde{H} as six first-order equations. We introduce six functions as

$$y_1 = \tilde{\eta}_{rrr}(\theta) = -\tilde{\eta}_{r\theta\theta}(\theta) = -\tilde{\eta}_{\theta r\theta}(\theta), \tag{A1}$$

$$y_2 = \tilde{\eta}_{rr\theta}(\theta), \tag{A2}$$

$$y_3 = \tilde{\eta}_{\theta\theta r}(\theta), \tag{A3}$$

$$y_4 = \tilde{\eta}_{\theta\theta\theta}(\theta) = -\tilde{\eta}_{\theta rr}(\theta) = -\tilde{\eta}_{r\theta r}(\theta), \tag{A4}$$

$$y_5 = \frac{d}{d\theta} \tilde{\eta}_{\theta\theta r}(\theta), \tag{A5}$$

$$y_6 = \tilde{H}(\theta), \tag{A6}$$

where $\tilde{\eta}_{\alpha\beta\gamma}(\theta)$ are the angular functions of strain gradients $\eta_{\alpha\beta\gamma}$. The functions y_i ($i = 1, 5$) are related to $\tilde{\phi}$, so the elimination of $\tilde{\phi}$ yields the following four relations,

$$\frac{dy_1}{d\theta} = y_2 - py_4, \tag{A7}$$

$$\frac{dy_2}{d\theta} = -(p + 1)y_1, \tag{A8}$$

$$\frac{dy_3}{d\theta} = y_5, \tag{A9}$$

$$\frac{dy_4}{d\theta} = 2y_1 - (p - 1)y_3. \tag{A10}$$

The equilibrium equations (39) give two additional equations for y_i ($i = 1, 6$). Therefore, we

have obtained a complete set of six first-order equations. The traction-free boundary conditions (41) on the crack face ($\theta = \pi$) can be written in terms of y_i ($i = 1, 6$).

In mode I fracture, the symmetry conditions (42) at $\theta = 0$ requires

$$y_2 = y_4 = y_5 = 0 \quad \text{at } \theta = 0. \quad (\text{A11})$$

A numerical shooting method iteratively assumes the initial value of other three variables, i.e. $y_1(\theta = 0)$, $y_3(\theta = 0)$ and $y_6(\theta = 0)$, until the traction-free boundary conditions (40) on the crack face are met. However, since this is an eigenvalue problem, we can impose a normalization condition

$$[y_1(\theta = 0)]^2 + [y_3(\theta = 0)]^2 + [y_6(\theta = 0)]^2 = 1, \quad (\text{A12})$$

which can be equivalently written as

$$y_1(\theta = 0) = \sin \alpha \sin \beta, \quad y_3(\theta = 0) = \sin \alpha \cos \beta, \quad y_6(\theta = 0) = \cos \alpha, \quad (\text{A13})$$

where α is a shooting parameter between 0 and 90° , while β is another shooting parameter between 0 and 360° . Since the power has been determined in Eq. (44) from the J -integral, two parameters α and β are determined iteratively to meet three traction-free boundary conditions (40) on the crack face ($\theta = \pi$). Our numerical results give the solutions of α and β in mode I as

$$\alpha = 86.56^\circ, \beta = 358.61^\circ \text{ or } \alpha = 88.61^\circ, \beta = 314.30^\circ \quad \text{for } l_1 = \frac{l}{16}, l_2 = \frac{l}{2}, l_3 = \sqrt{\frac{5}{24}}l \quad (\text{A14})$$

$$\alpha = 86.01^\circ, \beta = 358.76^\circ \text{ or } \alpha = 86.91^\circ, \beta = 312.12^\circ \quad \text{for } l_1 = \frac{l}{8}, l_2 = \frac{l}{2}, l_3 = \sqrt{\frac{5}{24}}l, \quad (\text{A15})$$

$$\alpha = 80.68^\circ, \beta = 267.82^\circ \quad \text{for } l_1 = l_2 = l_3 = \frac{l}{2}. \quad (\text{A16})$$

References

- [1] Ellsner G, Korn D, Rühle M. The influence of interface impurities on fracture energy of UHV diffusion bonded metal-ceramic bicrystals. *Scripta Metall Mater* 1994;31:1037–42.
- [2] Hutchinson JW. Linking scales in fracture mechanics. In: Karihaloo BL, Mai Y-W, Ripley MI, Ritchie RO, editors. *Advances in fracture research*. Amsterdam: Pergamon, 1997. p. 1–14.
- [3] Fleck NA, Hutchinson JW. A phenomenological theory for strain gradient effects in plasticity. *J Mech Phys Solids* 1993;41:1825–57.
- [4] Fleck NA, Hutchinson JW. Strain gradient plasticity. In: Hutchinson JW, Wu TY, editors. *Advances in applied mechanics*, 33. New York: Academic Press, 1997. p. 295–361.
- [5] Fleck NA, Muller GM, Ashby MF, Hutchinson JW. Strain gradient plasticity: theory and experiment. *Acta Metall Mater* 1994;42:475–87.
- [6] Gao H, Huang Y, Nix WD, Hutchinson JW. Mechanism-based strain gradient plasticity, Part I: theory. *J Mech Phys Solids* 1999;47:1239–63.

- [7] Huang Y, Gao H, Nix WD, Hutchinson JW. Mechanism-based strain gradient plasticity, Part II: analysis. *J Mech Phys Solids* 1999;48:99–128.
- [8] Nix WD. Mechanical properties of thin films. *Met Trans A* 1989;20A:2217–45.
- [9] De Guzman MS, Newbauer G, Flinn P, Nix WD. The role of indentation depth on the measured hardness of materials. *Materials Research Symposium Proceedings* 1993;308:613–8.
- [10] Stelmashenko NA, Walls AG, Brown LM, Milman YV. Microindentations on W and Mo oriented single crystals: an STM study. *Acta Metall et Mater* 1993;41:2855–65.
- [11] Ma Q, Clarke DR. Size dependent hardness of silver single crystals. *J Mater Res* 1995;10:853–63.
- [12] Poole WJ, Ashby MF, Fleck NA. Micro-hardness of annealed and work-hardened copper polycrystals. *Scripta Metall et Mater* 1996;34:559–64.
- [13] McElhaney KW, Vlassak JJ, Nix WD. Determination of indenter tip geometry and indentation contact area for depth-sensing indentation experiments. *J Mat Res* 1998;13:1300–6.
- [14] Stolken JS, Evans AG. A microbend test method for measuring the plasticity length scale. *Acta Mater* 1998;46:5109–15.
- [15] Nye JF. Some geometrical relations in dislocated crystals. *Acta Metall* 1953;1:153–62.
- [16] Cottrell AH. In: *The mechanical properties of materials*. New York: Wiley, 1964. p. 277.
- [17] Ashby MF. The deformation of plastically non-homogeneous alloys. *Phil Mag* 1970;21:399–424.
- [18] Huang Y, Zhang L, Guo TF, Hwang K-C. Near-tip fields for cracks in materials with strain gradient effects. In: Willis JR, editor. *IUTAM symposium on nonlinear analysis of fracture*. Dordrecht: Kluwer Academic Publishers, 1995. p. 231–43.
- [19] Huang Y, Zhang L, Guo TF, Hwang KC. Mixed mode near-tip fields for cracks in materials with strain gradient effects. *J Mech Phys Solids* 1997;45:439–65.
- [20] Xia ZC, Hutchinson JW. Crack tip fields in strain gradient plasticity. *J Mech Phys Solids* 1996;44:1621–48.
- [21] Chen JY, Huang Y, Hwang KC. Mode I and mode II plane-stress near-tip fields for cracks in materials with strain gradient effects. *Key Eng Mats* 1998;145:19–28.
- [22] Huang Y, Chen JY, Guo TF, Zhang L, Hwang KC. Analytical and numerical studies on mode I and mode II fracture in elastic–plastic materials with strain gradient effects, *Int. J. Fracture*. 1999 (in press).
- [23] Huang Y, Zhang L, Guo TF, Hwang K-C. Fracture of materials with strain gradient effects. In: Karihaloo BL, Mai Y-W, Ripley MI, Ritchie RO, editors. *Advances in fracture research*. Amsterdam: Pergamon, 1997. p. 2275–86.
- [24] Huang Y, Hwang KC, Guo TF. Fracture of materials at the microscale. In: Senoo M, Xu BY, Tokuda M, Bundara B, editors. *Mechanical problems of advanced engineering materials*. Mie University, Tsu, Japan: Mie University Press, 1998. p. 3–12.
- [25] Smyshlyaev VP, Fleck NA. The role of strain gradients in the grain size effect for polycrystals. *J Mech Phys Solids* 1996;44:465–95.
- [26] Rice JR. A path-independent integral and the approximate analysis of strain concentration by notches and cracks. *J Appl Mech* 1968;35:379–86.
- [27] Nix WD, Gao H. Indentation size effects in crystalline materials: a law for strain gradient plasticity. *J Mech Phys Solids* 1998;46:411–25.
- [28] Begley MR, Hutchinson JW. The mechanics of size-dependent indentation. *J Mech Phys Solids* 1998;46:2049–68.
- [29] Shu JY, Fleck NA. The prediction of a size-effect in microindentation. *Int J Solids structures* 1998;35:1363–83.
- [30] Hutchinson JW. Singular behavior at the end of a tensile crack in a hardening material. *J Mech Phys Solids* 1968;16:13–31.
- [31] Rice JR, Rosengren GF. Plane strain deformation near a crack tip in a power law hardening material. *J Mech Phys Solids* 1968;16:1–12.
- [32] Chen JY. *Fracture mechanics for materials with strain gradient effects*, Ph.D dissertation, (1998) Michigan Technological University, Houghton, MI 49931.
- [33] Wei Y, Hutchinson JW. On finite element method for the mixed strain problems 1999 (in preparation).
- [34] Shi MX, Huang Y, Hwang KC. Fracture in the higher order elastic continuum. 1999 (submitted for publication).

- [35] Wei Y, Hutchinson JW. Steady-state crack growth and work of fracture for solids characterized by strain gradient plasticity. *J Mech Phys Solids* 1997;45:1253–73.
- [36] Rice JR, Sih GC. Plane problems of cracks in dissimilar media. *J Appl Mech* 1965;32:418–23.
- [37] Press WH, Flannery BP, Teukolsky SA, Vetterling WT. *Numerical recipes*. Cambridge, UK: Cambridge University Press, 1986.